Nanoparticle Migration and Delivery of Paclitaxel to Regional Lymph Nodes in a Large Animal Model

Onkar V Khullar, MD[1], **Aaron P Griset, PhD**[2], **Summer L Gibbs-Strauss, PhD**[3], **Lucian R Chirieac, MD**[4], **Kimberly AV Zubris, BS**[2], **John V Frangioni, MD, PhD**[3], **Mark W Grinstaff, PhD**[2,*], and **Yolonda L Colson, MD, FACS**[1,*]

[1]Division of Thoracic Surgery, Brigham and Women's Hospital, Harvard Medical School, Boston, MA

[2]Departments of Biomedical Engineering and Chemistry, Boston University, Boston, MA

[3]Division of Hematology/Oncology, Beth Israel Deaconess Medical Center, Harvard Medical School, Boston, MA

[4]Department of Pathology, Brigham and Women's Hospital, Harvard Medical School, Boston, MA

Abstract

Background—To demonstrate feasibility of migration and *in situ* chemotherapy delivery to regional lymph nodes (LN) in a large animal model using an expansile polymer nanoparticle (eNP) delivery system.

Study Design—Dual-labeled 50 nm and 100 nm eNP were prepared by encapsulating an IR-813 near-infrared (NIR) fluorescent dye within coumarin-conjugated expansile polymer nanoparticles (NIR-C-eNP). NIR imaging and fluorescent microscopy were utilized to identify intralymphatic migration of NIR-nanoparticles to draining inguinal or mesenteric LN following injection in swine hindlegs or intestine. Nanoparticle-mediated intranodal delivery of chemotherapy was subsequently assessed with Oregon Green paclitaxel-loaded NIR-eNP (NIR-OGpax-eNP).

Results—NIR imaging demonstrated direct lymphatic migration of 50 nm, but not 100 nm, NIR-C-eNP and NIR-OGpax-eNP to the draining regional LNs following intradermal injection in the hindleg or subserosal injection in intestine. Fluorescent microscopy demonstrated that IR-813 used for NIR real-time trafficking colocalized with both the coumarin-labeled polymer and paclitaxel chemotherapy identified within the subcapsular spaces of the draining LNs. These studies verify nodal migration of both nanoparticle and encapsulated payload, and confirm the feasibility of focusing chemotherapy delivery directly to regional nodes.

Correspondence address: Yolonda L. Colson, MD, PhD, Division of Thoracic Surgery, Brigham and Women's Hospital, 75 Francis Street, Boston, MA 02115, ycolson@partners.org, Phone: (617) 732-6648, Fax: (617) 264-6878.
*Drs. Grinstaff and Colson have equally contributed to the conduct and oversight of this research.

Conclusions—Regionally-targeted intranodal chemotherapy can be delivered to draining LNs for both skin and solid organs using 50 nm paclitaxel-loaded eNP.

INTRODUCTION

Despite curative-intent at the time of tumor resection, many patients develop recurrent disease within regional lymph nodes (LN) hypothesized to result from "occult" micrometastatic disease missed at the initial surgery.[1–4] The clinical importance of unique tumor-specific lymphatic pathways used for the nodal migration of individual tumor cells was recognized in the identification of metastatic disease within "sentinel" lymph nodes (SLN), with SLN mapping now established as the standard of care in several malignancies, including melanoma and breast cancer.[5,6] Although metastases commonly occur via lymphatics, draining lymphatic channels and SLN have not been specifically targeted by adjuvant systemic chemotherapy.[7,8] When delivered systemically, concentrations of chemotherapy within the tumor and regional LN have been shown to be short-lived and 180–300 times lower than when delivered via lymphatics after peritumoral injection.[9] Due to various systemic drug toxicities and poor risk-to-benefit ratios for tumor prevention, adjuvant chemotherapy for early stage disease has not significantly prevented nodal recurrence nor has it demonstrated marked improvements in survival for many malignancies.[10,11] As such, targeted delivery of chemotherapy to draining LN at highest risk for harboring occult metastatic disease is particularly appealing for patients with early stage disease, since it serves as to increase intranodal drug concentrations, avoid systemic dose-limiting toxicities, and prevent growth of tumor hidden within the tumor-draining LN.

Although there is significant interest in the use of nanoparticle systems for intra-lymphatic drug transport[12–15], direct intranodal delivery of chemotherapy via dermal and visceral lymphatic pathways has not been documented using simultaneous, independent monitoring of both drug and nanoparticle in a large animal model where lymphatic anatomy and flow is more akin to humans. We have previously synthesized dynamic, pH-responsive expansile nanoparticles carrying the chemotherapeutic agent paclitaxel (Pax-eNP). When exposed to a mildly acidic environment (pH = 5), as with endocytosis by a tumor cell, Pax-eNP become hydrophilic, increase in volume, and release the encapsulated drug over 24 hours.[16] Moreover, a single treatment of Pax-eNP prevents establishment and delays recurrence in murine lung and mesothelioma cancer models, with superiority over conventional methods of paclitaxel delivery.[17,18] One of the main challenges in delivering chemotherapy via nanoparticles is the uncertainty that the drug and the nanoparticle are co-localizing. In this study, we independently assessed nanoparticle and drug lymphatic trafficking using multi-channel fluorescence. Using a large animal model for both cutaneous and solid organ lymphatic trafficking, real-time near-infrared (NIR) fluorescence imaging and *ex vivo* fluorescent microscopy demonstrated intralymphatic migration of eNP to regional LN within 24 hours, along with concomitant intranodal delivery of paclitaxel *in situ*.

METHODS

Synthesis of Fluorescently Labeled eNP

Coumarin-labeled NIR eNP (NIR-C-eNP) containing the NIR fluorophore IR-813 were synthesized using methacrylate and coumarin co-monomers. Unlabeled eNP, and paclitaxel-loaded (1% wt/wt monomer) eNP were produced using Monomer 1(5-methyl-2-phenyl-[1,3]-5-dioxanylmethyl methacrylate) via the miniemulsion method previously reported and subsequently adapted for coumarin co-monomer preparation (Figure 1).[16,19]

For NIR-C-eNP, 50 mg monomer 1, 0.7 mg 1,4-O-methacryloylhydroquinone, and 0.5 mg coumarin comonomer were dissolved in 0.5 mL of dichloromethane. IR-813 (70 µg) was

dissolved in dimethylsulfoxide and added to the monomer/crosslinker mixture before addition to a 10 mM phosphate buffer containing 5 or 50 mg of sodium dodecyl sulfate for 100 nm and 50 nm nanoparticles, respectively. The solution was sonicated under an argon blanket and polymerized with aqueous ammonium persulfate and *N,N,N',N'*-tetramethylethylenediamine. NIR-C-eNP were dialyzed in the dark against a 5 mM, pH 8.0 phosphate buffer to remove excess surfactant and salts with final dye concentrations of 50 µM IR-813 and 1 mM coumarin. Oregon-Green (OG) paclitaxel NIR eNP (NIR-OGpax-eNP) were similarly prepared using 10 µg OG 488-paclitaxel (Invitrogen) resulting in a final OG-paclitaxel concentration of 3.8 µM. All other chemicals were purchased from Sigma Aldrich (St. Louis, MO).

Nanoparticle Size, Charge and Optical Property Characterization

Nanoparticle size was assessed via dynamic light scattering on a 90Plus particle sizing instrument (Brookhaven Instruments) and via scanning electron microscopy on a Zeiss Supra 40VP field emission SEM with particles sized determined using NIH ImageJ. Surface charge was measured in 10 mM pH 7.4 phosphate buffer using a ZetaPALS zeta potential analyzer (Brookhaven Instruments). Fluorescence spectra measurements used fiber-optic HR2000 (200–1100 nm) and USB2000FL (350–1000 nm) spectrometers (Ocean Optics, Dunedin, FL). Fluorescence excitation for coumarin and Oregon green was provided by a 375 ± 10 nm light emitting diode and a 770 ± 2 nm laser for IR-813.

Animals

All Animals were housed in an AAALAC-certified facility staffed by full-time veterinarians, with supervised use under an approved institutional protocol in accordance with IACUC Guidelines. Four to six month old female Yorkshire pigs (30–40 kg; E.M. Parson's and Sons, Hadley, MA) were acclimated 48 hours before receiving pre-intervention sedation with 4.4 mg/kg intramuscular Telazol (Fort Dodge Labs, Fort Dodge, IA). Anesthesia was administered with 2% isoflurane/balance O_2 after intubation. At study completion, anesthetized animals were euthanized by a rapid injection of Fatal-Plus (Vortech Pharmaceuticals, Dearborn, MI), consistent with the AVMA Guidelines on Euthanasia.

In Vivo Nanoparticle Lymphatic Migration Analysis

One of three eNP suspensions were injected intradermally (200 µL) into the hindleg of an anesthetized pig 10 cm distal to the most inferior nipple: 100 nm NIR-C-eNP (n = 4), 50 nm NIR-C-eNP (n = 5), or 50 nm NIR-OGpax-eNP (n = 7). 50 nm NIR-C-eNP (n = 5) were used in studies assessing solid organ migration by injection within the subserosa of the small intestine after laparotomy. The extent of lymphatic uptake and migration was imaged 24 hours after injection in the hindleg, and in real-time after intestinal subserosal injection using the Fluorescence Assisted Resection and Exploration (FLARE™) NIR imaging system as previously described.[20,21] Briefly, the imaging system employs two wavelength-isolated excitation sources, a 400–650 nm "white" light and 725–775 nm NIR fluorescent light permitting real-time display of simultaneous color video, NIR fluorescent, and merged images. Under intraoperative FLARE™ guidance, the fluorescent IR-813 encapsulant was visualized, the injection site and SLN identified, and SLN and non-fluorescing LN dissected and harvested from the same nodal basin for comparative analysis.

Lymph Node Histology and Fluorescent Microscopy

Excised LN were fixed in 2% paraformaldehyde for 4 hours, mounted in Tissue-Tek O.C.T. compound (Fisher Scientific, Pittsburg, PA), frozen in liquid nitrogen, and cryosectioned at 10 µm. Tissue sections were examined for fluorescence through a modified microscope with

custom designed optics for NIR fluorescence visualization, described previously.[22] Coumarin fluorescence was visualized with excitation/emission filters of 360 ± 20 nm and 525 ± 25 nm, Oregon-Green at 480 ± 20 nm and 535 ± 30 nm andIR-813at 750 ± 25 nm and 810 ± 20 nm, respectively. Following fluorescence imaging, the same section was stained with hematoxylin and eosin. For qualitative colocalization analysis, fluorescence images of the different signals were pseudocolored with Adobe Photoshop CS4 to create color overlaid images. The percentage of colocalization was determined using NIH ImageJ software with the "Mander's Coefficient" plugin.[23]

RESULTS

Dual-labeled NIR Nanoparticles Exhibit Independent Fluorescent Signals for Polymer and Payload

We have previously demonstrated pH-triggered eNP expansion and slow release of encapsulated drug, along with rapid Pax-eNP entrance into tumor cells and potent *in vivo* tumor cytotoxicity.[16,18] Given these characteristics, we hypothesized that Pax-eNP would be well suited for intranodal drug delivery with the goal that once eNP arrived at the node, paclitaxel would be delivered directly into the subcapsular space where micrometastases are commonly found. To test this hypothesis, we created dual-labeled NIR-C-eNP by incorporating a coumarin comonomer into the polymer backbone (Figure 1a) along with encapsulation of the NIR-fluorescent dye IR-813 (Figure 1b) as payload. This would permit separate identification of the encapsulated payload and the nanoparticle itself during i*n vivo* lymphatic migration studies. Incorporation of these fluorescent labels into the nanoparticles did not alter the spectral properties of the fluorophores (coumarin λ at 450 and 490 nm and IR-813 λ at 847 nm; Figure 1d). For studies evaluating intranodal delivery of chemotherapy, paclitaxel fluorescently labeled with Oregon-Green (OGpax, Figure 1c) was encapsulated within eNP along with IR-813 (NIR-OGpax-eNP). The fluorescence spectrum of the NIR-OGpax-eNP shows peaks at 522 nm and 849 nm corresponding to OGpax and IR-813, respectively, allowing independent identification of each encapsulant (Figure 1e).

Intradermal Lymphatic Migration of Expansile Nanoparticles *In Vivo* in a Large Animal

As proof of concept for lymphatic delivery in a large animal approaching the size of humans, 50 nm NIR-C-eNP were injected intradermally into the hindlegs of Yorkshire pigs. Transcutaneous NIR fluorescent identification of the injection site and a discrete lymphatic channel between injection site and draining LN were observed in all animals. Figure 2 shows NIR-C-eNP lymphatic migration and LN accumulation 24 hours following intradermal injection (n = 5). In all pigs, 1 to 3 discrete fluorescent LN were readily identified transcutaneously within the regional draining lymphatic basin and were subsequently excised under NIR guidance (Figure 2, bottom). Although several LN were contained with the same nodal basin, lymphatic drainage from the injection site was specific to discrete LN within that nodal group, with the other nodes thus serving as negative controls.

In order to assess the impact of size and particle charge on the ability of eNP to enter and migrate within the lymphatic system, 100nm C-eNP were also synthesized and characterized. Particle sizes were measured and compared using dynamic light scattering (93.9 ± 1.00 nm and 48.1 ± 0.56; p < 0.0001). This was confirmed with SEM micrographs showing the morphology and size distribution of C-eNP, with average diameters of 105.4 ± 37.0 nm and 54.7 ± 34.6 nm, respectively (Figure 3). In addition to a larger size, 100 nm C-eNP exhibited a less negative zeta potential (−34.52 ± 0.46 mV) compared to the 50 nm C-eNP (−46.87 ± 0.94 mV; p < 0.0001). The polydisperity indexes for the particles were 0.117 ± 0.01 and 0.284 ± 0.01 respectively. These differences translated into a marked difference

in migratory ability 24 hours following intradermal injection of 100 nm NIR-C-eNP (n = 4). The entire NIR-IR-813 signal remained at the injection site, indicating that 100 nm NIR-C-eNP do not exhibit significant lymphatic migration during this time period. Presence of IR-813 signal within discrete regional LN following injection of 50nmNIR-C-eNP versus only at the injection site with 100nm NIR-C-eNP, confirmed that IR-813 was not prematurely released from eNP nor did it freely migrate within lymphatics. Instead, lymphatic migration of eNP and IR-813 payload occurred simultaneously.

In Vivo Nanoparticle-mediated Targeting of Visceral Draining Lymph Nodes in a Large Animal

To determine if lymphatic migration and nanoparticle-mediated nodal targeting is potentially applicable to solid organ malignancies, similar studies were performed following subserosal injection of 50 nm NIR-C-eNP in the intestine of Yorkshire pigs (n = 5). Animals were imaged immediately after injection with rapid migration evident within 30 seconds in all cases. Migration occurred via 1 to 3 discrete lymphatic channels, with all pathways subsequently coalescing into a single draining LN at the base of the mesentery (Figure 4). Migration of NIR-C-eNP to a discrete mesenteric LN was evident in all animals, confirming the feasibility of intra-operative nodal targeting.

Nanoparticle and NIR Encapsulant Colocalization within the Subcapsular Space of Draining Lymph Nodes

Regional draining LN were readily identified and harvested via NIR guidance following injection of 50nm, but not 100nm, NIR-C-eNP, leading to our hypothesis that IR-813 was delivered to the regional LN via direct nanoparticle migration. To show that IR-813 co-migrated inside the node within 50 nm NIR-C-eNP, dual-image histologic analysis of NIR-positive LN was performed with a modified NIR fluorescence microscope, allowing for independent assessment of IR-813 and coumarin-labeled polymer *in situ*.[22] As shown in Figure 5, using H&E staining to identify corresponding nodal architecture (5a), encapsulated IR-813 (5b: red) and coumarin-labeled eNP (5c: green) signals colocalized within the LN on merged images (5d: yellow). Colocalization was determined, independent of fluorescence intensity, using Mander's overlap coefficients[23] and demonstrated almost uniform colocalization of IR-813 and coumarin signals (0.938 ± 0.023) thereby confirming that the encapsulant migrated with eNP through the draining lymphatics into the node, rather than via nanoparticle release at the point of injection.

Expansile Nanoparticles Deliver Paclitaxel to Draining Lymph Nodes

To determine intranodal delivery of chemotherapy, paclitaxel fluorescently labeled with Oregon-Green was encapsulated within 50 nm eNP along with IR-813 (NIR-OGpax-eNP). Coumarin labeling of the polymer was not utilized due to overlapping fluorescent spectra of OG-Pax and coumarin moieties. NIR-OGpax-eNP was administered via an intradermal hindleg injection and NIR fluorescence guided excision of the draining LN was performed 24 hours later. As with NIR-CeNP, lymphatic migration of NIR-OGpax-eNP was readily visible with identification and excision of a discrete draining lymph node under NIR guidance (Figures 6a & b). NIR and fluorescent microscopy verified direct intranodal paclitaxel delivery via NIR-OGpax-eNP by demonstrating co-localization of IR-813 and OG-Pax signals (Figures 6 d, e & f) within the subcapsular spaces of the LN *in situ* (Figure 6c), with an overlap coefficient of 0.945 ± 0.056. The absence of OG-Pax signal within NIR-negative control nodes within the same drainage basin, further established that OG-paclitaxel delivery was nanoparticle-mediated.

DISCUSSION

The overall goal of this study was to develop a nanoparticle-mediated drug delivery system in which chemotherapy delivery was targeted to tumor-draining regional LN, which are susceptible to recurrent disease following surgical resection of an otherwise locally confined malignancy. Similar to our findings in this large animal model, several studies in rodents have identified the acceptable nanoparticle size required for lymphatic transport to be between 10 – 100 nm[24–28], with Reddy et al demonstrating the greatest rate of LN uptake and retention within the 20 – 45 nm range.[28] As we found with 100 nm eNP, larger particles typically remain confined to the injection site, whereas nanoparticles smaller than 10 nm diffuse into capillaries and escape LN capture. Other studies have characterized additional promigratory criteria using PLGA [poly(lactic-*co*-glycolic acid)] nanoparticles, with migration and nodal retention directly related to anionic charge with less particle aggregation and greater lymphatic uptake.[28–31] Similarly, rapid lymphatic migration of 50 nm NIR-C-eNP, which are both smaller in size and have a more negative zeta potential than the nonmigratory 100 nm NIR-C-eNP (Figure 3), indicates that these criteria also hold true for eNP migration within the lymphatics of large animals.

Previous investigators, using drug-loaded PLA or PLGA nanoparticles in rodent models, have used HPLC to detect the presence of encapsulated chemotherapy within LNs.[32,33] However, specificity of drug delivery to individual draining LNs and the presence of nanoparticles specifically within the subcapsular spaces of those nodes have not been demonstrated. In fact, after pleural implantation of a gelatin sponge containing paclitaxel-loaded PLGA nanoparticles, Liu et al detected paclitaxel in both ipsilateral and contralateral mediastinal lymph nodes, indicating more generalized, and non-targeted, drug delivery.[33] Such bilateral or systemic drug detection suggests that paclitaxel delivery may not be concentrated within draining nodes, as seen with NIR-OGpax-eNP, but rather may occur diffusely and independent of nodal migration of the nanoparticle.

Direct nanoparticle-mediated intranodal delivery in an *in vivo* pre-clinical large animal model, for either cutaneous or solid organ systems, has not been shown and is a necessary step for potential clinical application of this technology. In order to demonstrate focused chemotherapy delivery using a nanoparticle-drug delivery system to LN specifically draining a tumor bed, independent monitoring of nanoparticle and encapsulant is required. Consequently, the NIR dye IR-813 was encapsulated within eNP in which either a) the polymer was fluorescently labeled for later histologic identification or b) contained OG-Pax as a co-encapsulant for subsequent histologic localization of drug delivery. We chose to utilize nonradioactive NIR imaging for these studies as it is ideal for real-time intra-operative lymphatic mapping and visualization through intact skin or mesentery due to its low autofluorescence in biologic tissues and fluids.[34–36] NIR mapping using ICG has previously been shown to be an effective means of accurately identifying sentinel lymph nodes.[20] Given that sentinel lymph node identification via NIR was equivalent to using radioactive tracers, we have leveraged the safety of NIR imaging for lymphatic mapping in these studies. As confirmed by colocalization of IR-813 and coumarin on histologic analysis of NIR positive nodes, IR-813 permitted real-time identification of nanoparticle location *in situ* for both subdermal and submucosal lymphatics, a clinically useful approach to the monitoring of nanoparticle trafficking. While a significant amount of fluorescence remained at the injection site at 24 hours, given the size and charge of the particle we would expect continued migration to the regional nodes over time, which will be the subject of future studies. Similarly, use of fluorescently-labeled OG-Pax allowed independent analysis of intranodal nanoparticle vs. drug distribution *in situ*, with both being delivered to the subcapsular space of the node. This intranodal location makes biologic and oncologic sense as the subcapsular space lies immediately beneath the LN capsule, communicates with the

afferent lymphatic vessel, and most importantly, is where initial tumor metastases are found.[37–40] Analysis of nodal pathology in melanoma demonstrated that 86% of tumor metastases were within the subcapsular space[38], making this a prime intranodal location for delivery of chemotherapeutics directed against occult nodal disease. Studies of other nanoparticle formulations have shown a similar subcapsular distribution on histologic analysis of nearby nodes following interstitial or footpad injection[26,28], suggesting that nanoparticle delivery may be particularly well-suited to nodal-targeted drug delivery.

In summary, we have developed a lymphatic drug delivery system using pH-responsive, expansile nanoparticles whereby encapsulated chemotherapy is carried by regional lymphatics to the draining nodes that, in the presence of a tumor, are most at risk for nodal metastases. The encapsulation of the NIR dye IR-813 has allowed real-time *in situ* monitoring of nanoparticle trafficking, identification of targeted nodes and confirmation of intranodal nanoparticle-mediated delivery of paclitaxel. Furthermore, eNP-mediated delivery of paclitaxel occurred in the subcapsular spaces of the LN, a common location for occult micrometastatic disease. These results demonstrate feasibility in a large animal model and suggest that nanoparticle-mediated drug delivery may potentially play a future role in targeted approaches aimed at the prevention and treatment of early occult metastatic disease in regional LNs. This study warrants future longterm investigation in large animals in order to elucidate the kinetics of intranodal nanoparticle migration and excretion over longer periods of time, to assess chemotherapy delivery throughout the entire lymph node chain, to determine the efficacy of intra-lymphatic drug therapy, and to assess for long term toxicity of these particles.

Acknowledgments

References

1. Wu J, Ohta Y, Minato H, et al. Nodal occult metastasis in patients with peripheral lung adenocarcinoma of 2.0 cm or less in diameter. Ann Thorac Surg. 2001; 71:1772–1777. [PubMed: 11426746]

2. de Boer M, van Deurzen CH, van Dijck JA, et al. Micrometastases or isolated tumor cells and the outcome of breast cancer. N Engl J Med. 2009; 361:653–663. [PubMed: 19675329]

3. Gershenwald JCM, Lee J, et al. Patterns of recurrence following a negative sentinel lymph node biopsy in 243 patients with stage I or II melanoma. J Clin Oncol. 1998; 16:2253–2260. [PubMed: 9626228]

4. Takeuchi H, Kitajima M, Kitagawa Y. Sentinel lymph node as a target of molecular diagnosis of lymphatic micrometastasis and local immunoresponse to malignant cells. Cancer Sci. 2008; 99:441–450. [PubMed: 18070155]

5. Morton DL, Cochran AJ, Thompson JF, et al. Sentinel node biopsy for early-stage melanoma: accuracy and morbidity in MSLT-I, an international multicenter trial. Ann Surg. 2005; 242:302–311. [PubMed: 16135917]

6. Chen SL, Iddings DM, Scheri RP, Bilchik AJ. Lymphatic mapping and sentinel node analysis: current concepts and applications. CA Cancer J Clin. 2006; 56:292–309. [PubMed: 17005598]

7. Pepper MS. Lymphangiogenesis and tumor metastasis: myth or reality? Clin Cancer Res. 2001; 7:462–468. [PubMed: 11297234]

8. Van Trappen PO, Pepper MS. Lymphatic dissemination of tumour cells and the formation of micrometastases. Lancet Oncol. 2002; 3:44–52. [PubMed: 11905605]

9. Chen J, Wang L, Yao Q, et al. Drug concentrations in axillary lymph nodes after lymphatic chemotherapy on patients with breast cancer. Breast Cancer Res. 2004; 6:R474–R477. [PubMed: 15217515]

10. Benson AB, Schrag D, Somerfield MR, et al. American Society of Clinical Oncology recommendations on adjuvant chemotherapy for stage II colon cancer. J Clin Oncol. 2004; 22:3408–3419. [PubMed: 15199089]

11. Pisters KMW, Evans WK, Azzoli CG, et al. Cancer Care Ontario and American Society of Clinical Oncology adjuvant chemotherapy and adjuvant radiation therapy for stages IIIA resectable non–small-cell lung cancer guideline. J Clin Oncol. 2007; 25:5506–5518. [PubMed: 17954710]

12. Duncan R. Polymer conjugates as anticancer nanomedicines. Nat Rev Cancer. 2006; 6:688–701. [PubMed: 16900224]

13. Torchilin VP. Multifunctional nanocarriers. Adv Drug Deliv Rev. 2006; 58:1532–1555. [PubMed: 17092599]

14. Kabanov AV. Polymer genomics: An insight into pharmacology and toxicology of nanomedicines. Adv Drug Deliv Rev. 2006; 58:1597–1621. [PubMed: 17126450]

15. Davis ME, Chen ZG, Shin DM. Nanoparticle therapeutics: an emerging treatment modality for cancer. Nat Rev Drug Discov. 2008; 7:771–782. [PubMed: 18758474]

16. Griset AP, Walpole J, Liu R, et al. Expansile nanoparticles: synthesis, characterization, and in vivo efficacy of an acid-responsive polymeric drug delivery system. J Am Chem Soc. 2009; 131:2469–2471. [PubMed: 19182897]

17. Colson YLLR, Southard EB, Schulz MD, et al. The performance of expansile nanoparticles in a murine model of peritoneal carcinomatosis. Biomaterials. 2011; 32:832–840. [PubMed: 21044799]

18. Liu R, Khullar OV, Griset AP, et al. Paclitaxel-loaded expansile nanoparticles delay local recurrence in a heterotopic murine non-small cell lung cancer model. Ann Thorac Surg. 2011; 91:1077–1083. discussion 1083–1084. [PubMed: 21440127]

19. Zubris KAKO, Griset AP, Gibbs-Strauss S, et al. Ease of synthesis, controllable sizes, and in vivo large-animal-lymph migration of polymeric nanoparticles. Chem Med Chem. 2010; 5:1435–1438. [PubMed: 20593440]

20. Troyan S, Kianzad V, Gibbs-Strauss S, et al. The FLARE™ intraoperative near-infrared fluorescence imaging system: A first-in-human clinical trial in breast cancer sentinel lymph node mapping. Ann Surg Oncol. 2009; 16:2943–2952. [PubMed: 19582506]

21. Gioux S, Kianzad V, Ciocan R, et al. High-power, computer-controlled, light-emitting diode-based light sources for fluorescence imaging and image-guided surgery. Mol Imaging. 2009; 8:156–165. [PubMed: 19723473]

22. Zaheer A, Lenkinski RE, Mahmood A, et al. In vivo near-infrared fluorescence imaging of osteoblastic activity. Nat Biotechnol. 2001; 19:1148–1154. [PubMed: 11731784]

23. Manders EEM, Verbeek FJ, Aten JA. Measurement of co-localisation of objects in dual-colour confocal images. J Microscopy. 1993; 169:375–382.

24. Hawley AE, Davis SS, Illum L. Targeting of colloids to lymph nodes: Influence of lymphatic physiology and colloidal characteristics. Adv Drug Deliv Rev. 1995; 17:129–148.

25. Oussoren C, Storm G. Liposomes to target the lymphatics by subcutaneous administration. Adv Drug Deliv Rev. 2001; 50:143–156. [PubMed: 11489337]

26. Manolova V, Flace A, Bauer M, et al. Nanoparticles target distinct dendritic cell populations according to their size. Eur J Immunol. 2008; 38:1404–1413. [PubMed: 18389478]

27. Xie Y, Bagby TR, Cohen M, Forrest ML. Drug delivery to the lymphatic system: Importance in future cancer diagnosis and therapies. Expert Opin Drug Deliv. 2009

28. Reddy ST, Rehor A, Schmoekel HG, et al. In vivo targeting of dendritic cells in lymph nodes with poly(propylene sulfide) nanoparticles. J Control Release. 2006; 112:26–34. [PubMed: 16529839]

29. Hawley AE, Illum L, Davis SS. Preparation of biodegradable, surface engineered PLGA nanospheres with enhanced lymphatic drainage and lymph node uptake. Pharm Res. 1997; 14:657–661. [PubMed: 9165539]

30. Kaminskas LM, Kota J, McLeod VM, et al. PEGylation of polylysine dendrimers improves absorption and lymphatic targeting following SC administration in rats. J Control Release. 2009; 140:108–116. [PubMed: 19686787]

31. Rao DA, Forrest ML, Alani AW, et al. Biodegradable PLGA based nanoparticles for sustained regional lymphatic drug delivery. J Pharm Sci. 2010; 99:2018–2031. [PubMed: 19902520]

32. Lu HX, Li B, Kang Y, et al. Paclitaxel nanoparticle inhibits growth of ovarian cancer xenografts and enhances lymphatic targeting. Cancer Chemother Pharmacol. 2007; 59:175–181. [PubMed: 16718469]

33. Liu J, Meisner D, Kwong E, et al. Translymphatic chemotherapy by intrapleural placement of gelatin sponge containing biodegradable paclitaxel colloids controls lymphatic metastasis in lung cancer. Cancer Res. 2009; 69:1174–1181. [PubMed: 19176391]

34. Frangioni JV. In vivo near-infrared fluorescence imaging. Curr Opin Chem Biol. 2003; 7:626–634. [PubMed: 14580568]

35. Makino A, Kizaka-Kondoh S, Yamahara R, et al. Near-infrared fluorescence tumor imaging using nanocarrier composed of poly(L-lactic acid)-block-poly(sarcosine) amphiphilic polydepsipeptide. Biomaterials. 2009; 30:5156–5160. [PubMed: 19525007]

36. Khullar O, Frangioni JV, Grinstaff M, Colson YL. Image-guided sentinel lymph node mapping and nanotechnology-based nodal treatment in lung cancer using invisible nearinfrared fluorescent light. Semin Thorac Cardiovasc Surg. 2009; 21:309–315. [PubMed: 20226343]

37. Carr I. Lymphatic metastasis. Cancer Metastasis Rev. 1983; 2:307–317. [PubMed: 6367969]

38. Murray CA, Leong WL, McCready DR, Ghazarian DM. Histopathological patterns of melanoma metastases in sentinel lymph nodes. J Clin Pathol. 2004; 57:64–67. [PubMed: 14693838]

39. Dewar DJ, Newell B, Green MA, et al. The microanatomic location of metastatic melanoma in sentinel lymph nodes predicts nonsentinel lymph node involvement. J Clin Oncol. 2004; 22:3345–3349. [PubMed: 15310779]

40. van Deurzen CH, Seldenrijk CA, Koelemij R, et al. The microanatomic location of metastatic breast cancer in sentinel lymph nodes predicts nonsentinel lymph node involvement. Ann Surg Oncol. 2008; 15:1309–1315. [PubMed: 18253802]
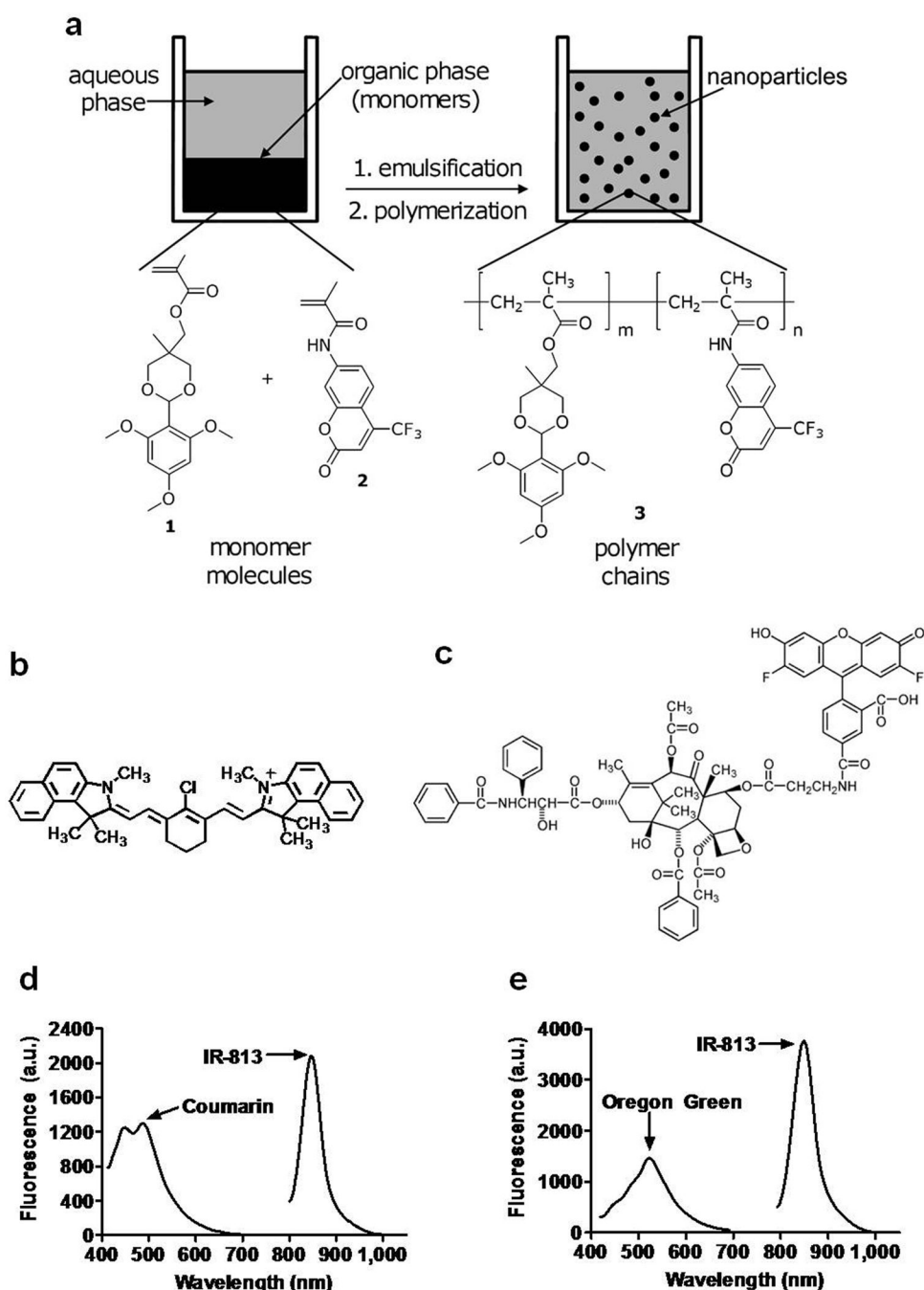
Figure 1.
Structural and fluorescent properties of IR-813 encapsulated in coumarin-eNP: (a) An emulsion of an acrylate monomer possessing a 2,4,6-trimethoxybenzaldehyde protecting group (1) and a coumarin-6 co-monomer (2) was used to synthesize Coumarin labeled pH-responsive 50 and 100 nm nanoparticles (3). IR-813 (b) was encapsulated with or without Oregon Green paclitaxel (c) into unlabeled and coumarin-labeled eNP (NIR-OGpax-eNP and NIR-C-eNP, respectively) to create the two types of dual-labeled particles for subsequent trafficking studies. (d) Fluorescence spectrum of NIR-C-eNP (λexc = 375 ± 10 nm and 770 ± 2 nm). (e) Fluorescence spectrum of NIR-OGpax-eNP (λexc = 375 ± 10 nm and 770 ± 2 nm).
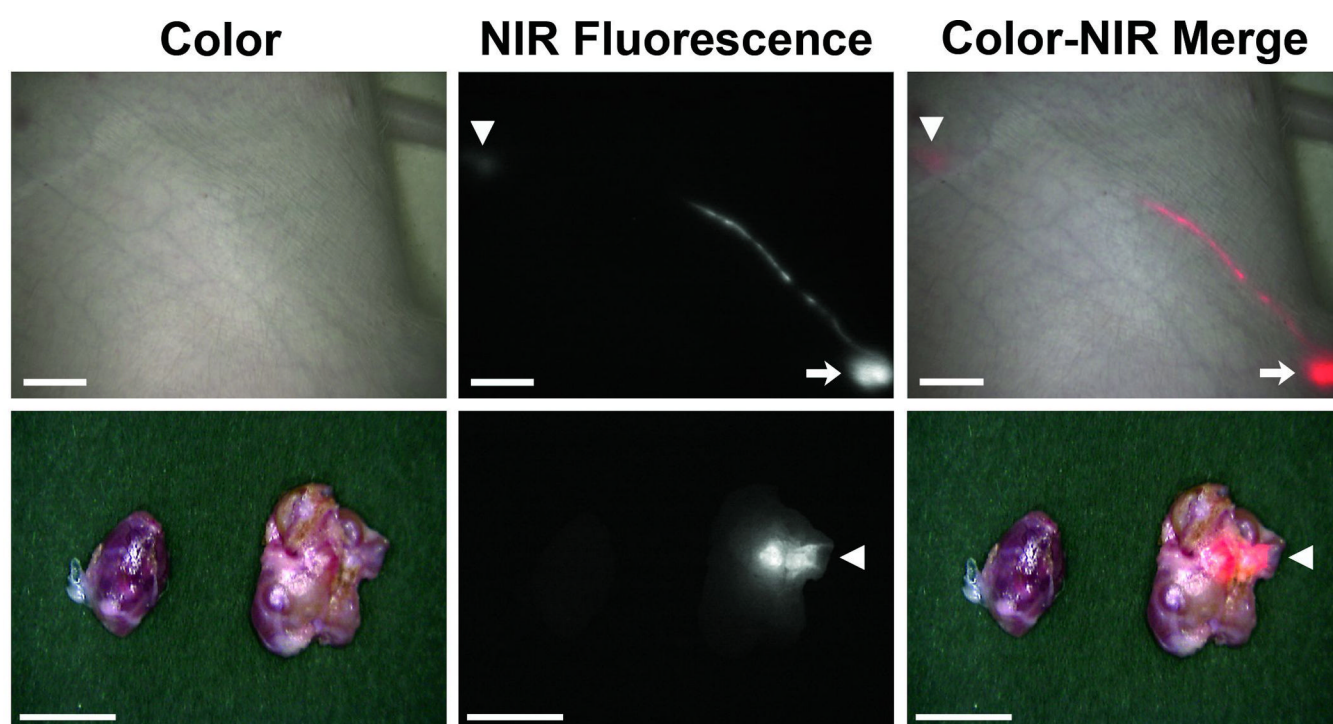
Figure 2.
In vivo NIR imaging of nanoparticle lymphatic migration: (Top) IR-813 encapsulated eNP are seen migrating from the site of injection (arrow) to a regional draining lymph node (arrowhead) through a discrete lymphatic channel. Shown are representative color (left), NIR fluorescence (middle), and a pseudocolored (red) merged (right) images, 24 hours after injection. Scale bar = 1 cm.(Bottom) Using real-time, intraoperative NIR image guidance, the specific draining lymph node is identified and distinguished from adjacent non-draining LNs. Shown are representative images of the dissected, fluorescent LN (right) and an adjacent non-draining node (left). Arrowhead marks sinus entry point. Scale bar = 0.5 cm.
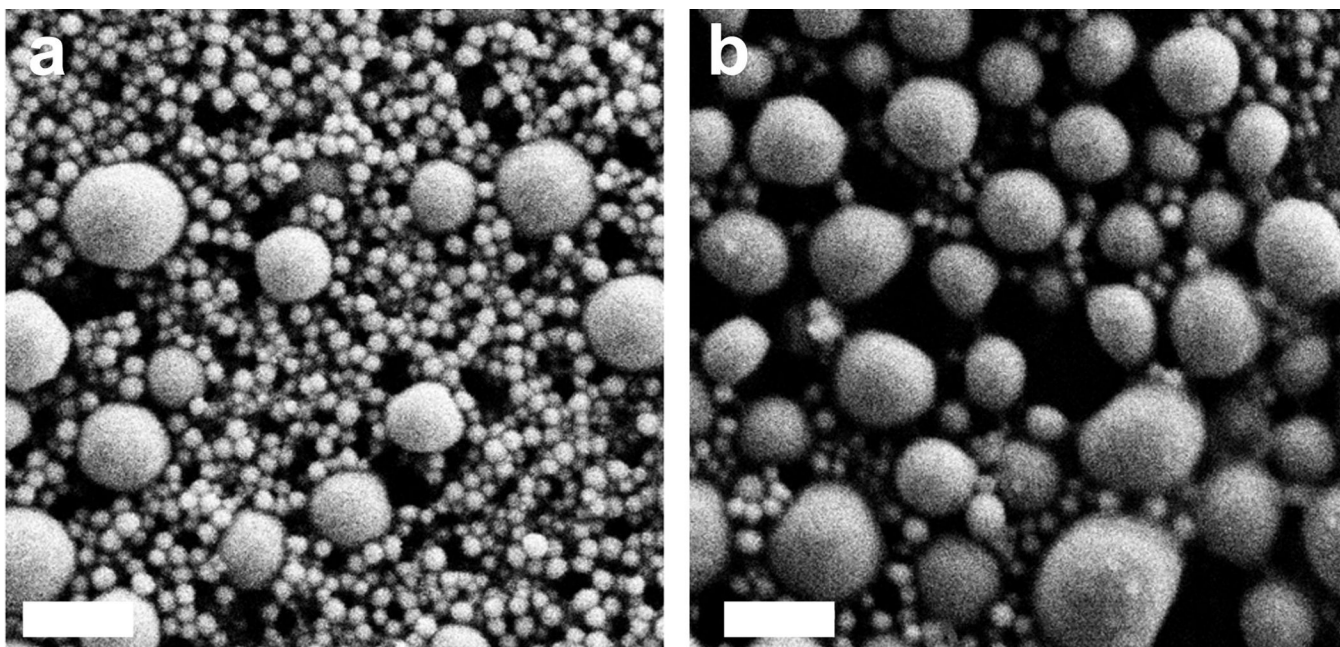
Figure 3.
Scanning electron micrographs of (a) 50 nm C-eNP and (b) 100 nm C-eNP. Scale bar = 200 nm.
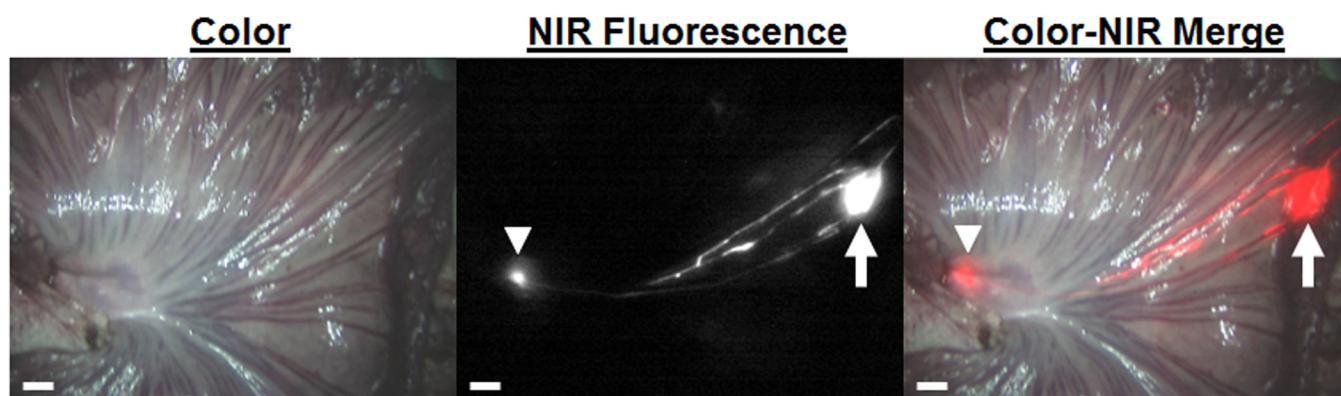
Figure 4.
In vivo nanoparticle lymphatic migration in pig intestine: 50 nm IR-813 encapsulated eNP are seen migrating from the subserosal injection site within the small bowel (arrow) through easily identifiable lymphatic channels to a single mesenteric draining lymph node (arrowhead). Shown are representative color (left), NIR fluorescence (middle), and a pseudo-colored (red) merged(right) images, 4 minutes after injection. Scale bar = 1 cm.
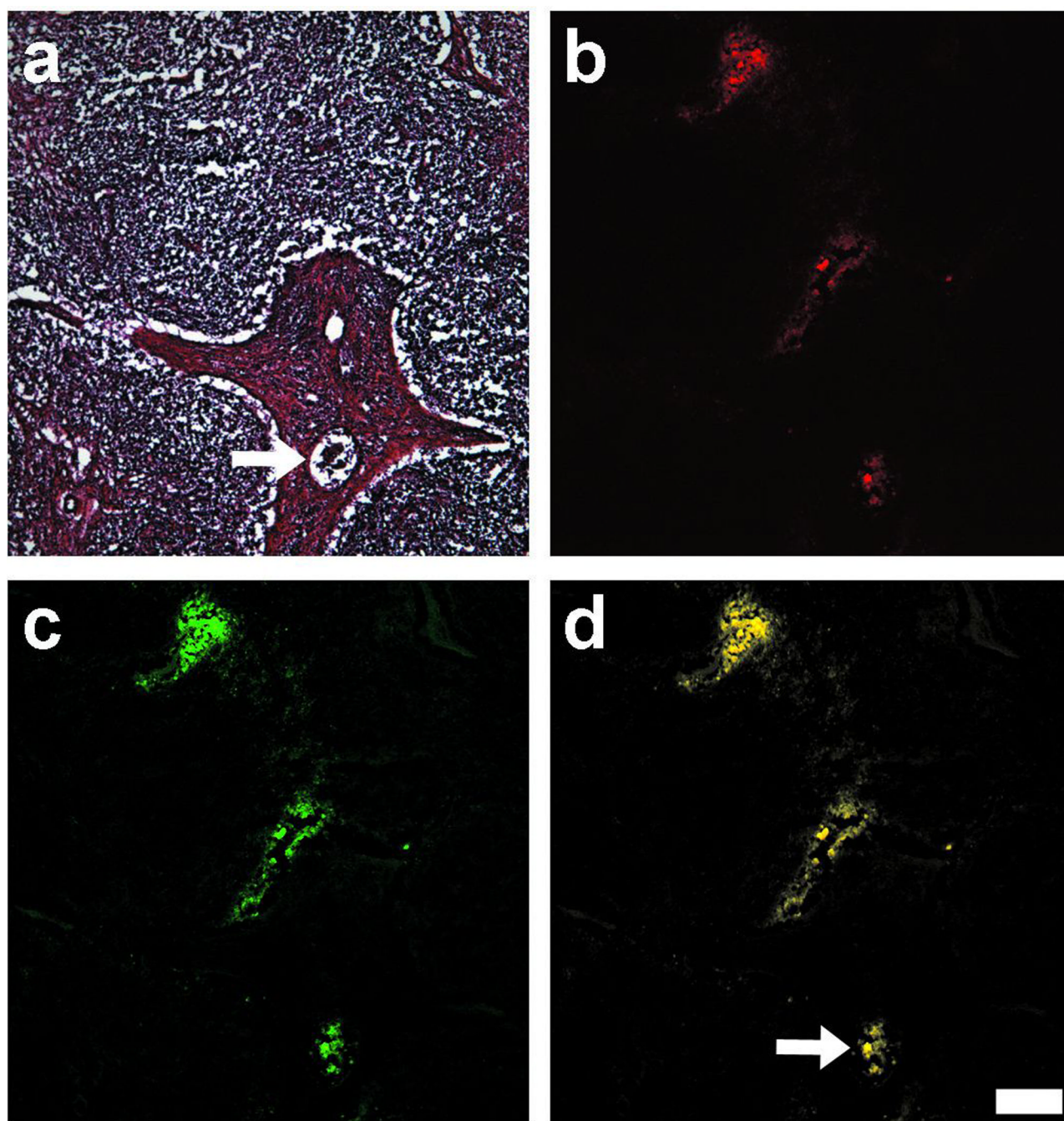
Figure 5.
Histologic analysis of SLN after intradermal injection of NIR-C-eNP: After SLN dissection and preparation of tissue frozen sections, histological images were prepared. Shown are (a) H & E, (b) NIR fluorescence of IR-813 payload (red), (c) coumarin fluorescence of eNP (green), and (d) pseudo-colored merged images confirming colocalization of IR-813 and coumarin ($R = 0.938 \pm 0.023$), as well as lymphatic migration of both the eNP and encapsulated dye to the SLN. The arrow highlights a lymphatic vessel containing fluorescence within the SLN. Scale bar = 200 µm.
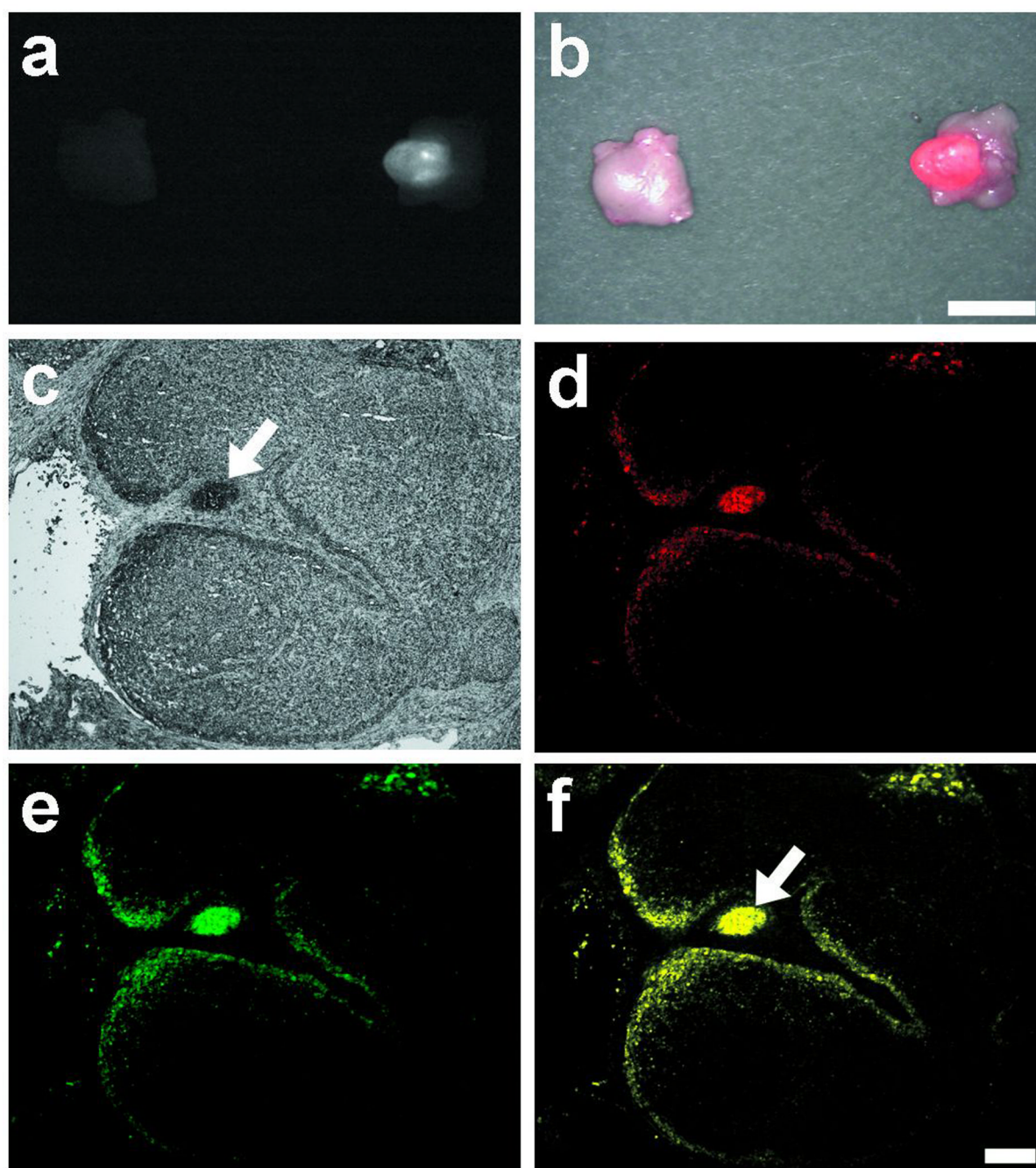
Figure 6.
IR-813 and Oregon Green-paclitaxel dual-encapsulated expansile nanoparticles: In vivo NIR imaging confirmed migration of the NIR-OGpax-eNP to a specific draining regional LN. Shown are NIR fluorescence (a) and pseudocolored (red) merged images(b) of the draining and nearby LN. Scale bar = 0.5 cm. Fluorescent microscopy confirmed eNP-mediated delivery of paclitaxel chemotherapy within the LN on histologic analysis. The following images are shown: (c) white light, (d) NIR fluorescence of IR-813 (red), (e) Oregon Green fluorescence of encapsulated paclitaxel (green), and (f) pseudocolored merged images. NIR-OGpax-eNP are visualized within an afferent lymphatic vessel (arrow). Scale bar = 200 µm.